The evolution of Luminous Red Galaxies in the Sloan Digital Sky Survey 7th data release

Rita Tojeiro*[1] and Will J. Percival[1]

[1] Institute of Cosmology and Gravitation, Dennis Sciama Building, University of Portsmouth, Burnaby Road, Portsmouth, PO1 3FX

5 March 2010

ABSTRACT

We present a comprehensive study of the evolution of Luminous Red Galaxies (LRGs) in the latest and final spectroscopic data release of the Sloan Digital Sky Survey. We test the scenario of passive evolution of LRGs in $0.15 < z < 0.5$, by looking at the evolution of the number and luminosity density of LRGs, as well as of their clustering. A new weighting scheme is introduced that allows us to keep a large number of galaxies in our sample and put stringent constraints on the growth and merging allowed by the data as a function of galaxy luminosity. Introducing additional luminosity-dependent weighting for our clustering analysis allows us to additionally constrain the nature of the mergers. We find that, in the redshift range probed, the population of LRGs grows in luminosity by 1.5-6 % Gyr^{-1} depending on their luminosity. This growth is predominantly happening in objects that reside in the lowest-mass haloes probed by this study, and cannot be explained by satellite accretion into massive LRGs, nor by LRG-LRG merging. We find that the evolution of the brightest objects (with a K+e-corrected $M_{r,0.1} \lesssim -22.8$) is consistent with that expected from passive evolution.

Key words: galaxies: evolution - cosmology: observations - surveys

1 INTRODUCTION

Luminous Red Galaxies (LRGs) are useful probes of large scale structure. They are bright and have the potential to be easily separated by colour, allowing a uniform sample to be selected with which to map large volumes. They are also strongly biased with respect to the matter distribution, making them particularly attractive for studies that aim to use Baryon Acoustic Oscillations (BAO) in the galaxy distribution to study the expansion of the Universe (Seo & Eisenstein 2003; Blake & Glazebrook 2003; Hu & Haiman 2003; Matsubara 2004). Because of this, LRGs are being targeted by the Baryon Oscillation Spectroscopic Survey (BOSS; Schlegel et al. 2009), part of the SDSS-III project, in order to map the expansion rate out to $z < 0.7$.

In addition to allowing measurements of cosmological expansion by using the BAO signal as a standard ruler, galaxy surveys also measure the growth of structure through redshift-space distortions (e.g., Kaiser 1987; Davis & Peebles 1983 and Hamilton 1998 for a review). Although current BAO and z-space distortion analyses are generally robust to an evolving galaxy bias, future experiments will be more sensitive to these effects (e.g. Smith et al.

2007). Observing a single population of passively evolving galaxies offers an attractive way of minimising bias effects. In particular, for such a sample, the redshift evolution of bias and its effects on cosmological probes can be more easily modelled. Uniformity in terms of selection is also advantageous for cosmological studies of large-scale structure, which are often simplified if the relationship between the galaxies and the underlying density field is uniform across the sample. It is therefore extremely interesting to ask whether a uniform, passively evolving population of galaxies can be found.

LRGs are the most likely candidate for such a sample, as they are traditionally assumed to form a single population of galaxies, which assembled at high-redshift and has been passively evolving since. As red galaxies dominate the stellar mass budget in the Universe, understanding how they assemble and grow is a key question in theories of galaxy formation and evolution. Driven both by galaxy evolution and observational cosmology, passive evolution of LRGs has been tested extensively. Traditionally, this is done by looking at three main observables and their evolution with redshift: the total comoving number density, the luminosity function and density, and the large or small-scale clustering.

Firstly and most simply, passive evolution predicts that the number density of objects must be conserved as a function of time. This has been tested by Wake et al. (2006), who

* E-mail: rita.tojeiro@port.ac.uk

found that the number density of LRGs brighter than a given luminosity is conserved between $z = 0.55$ and $z = 0.2$, if one accounts for the passive fading of the stellar populations.

Secondly, we can go further and look at the evolution of the luminosity density as a function of redshift. Wake et al. (2006) used the 2SLAQ sample to investigate whether the luminosity function (LF) at $z = 0.2$ and $z = 0.55$ is consistent with a purely passive evolution. They found that this is indeed the case. Furthermore, they also looked at the effect of major LRG-LRG mergers in the LF. They found that the observed LFs are fully consistent with a merger-free history. Brown et al. (2007), focusing on the B-band luminosity density, have found a slight departure from pure passive evolution, and that around 80% of the stellar mass in massive red galaxies ($> 4L^*$) today was already in place by $z = 0.7$. This results in a modest growth of $\approx 3\%$ Gyr^{-1} in mass or luminosity. Cool et al. (2008) put a similar limit on the growth of very bright red galaxies ($> 3L^*$), and showed that bright red galaxies can not have grown by more than 50% since $z = 0.9$, or $\approx 6.8\%$ Gyr^{-1}.

These studies face a fundamental problem that, while we can match numbers of objects and the luminosity function to those expected for a particular evolutionary theory, we cannot test whether this is a coincidence. The match is necessary to test the theory, but is not sufficient to show that the theory must be true. In particular, for passive evolution, one can potentially have galaxies entering and/or leaving the red sequence at any point during the tested timeline, and several effects can change the number or luminosity density of a sample. This can happen by:

(i) blue galaxies quenching star formation and becoming red;

(ii) fainter red galaxies merging together without triggering star formation (SF) to enter the sample at lower redshift;

(iii) LRGs merging with other LRGs to decrease the number density at low redshift

(iv) LRGs leaving the red-sequence due to merger-induced SF.

The lack of massive blue galaxies makes i) and iv) weak propositions. Furthermore, LRG-LRG mergers tend to be dry, given that massive red galaxies have little in the way of gas and SF. But ii) and iii) almost certainly play a role in the overall LRG population evolution. The question is: how much so?

One can hope to distinguish between these scenarios by investigating the clustering of the LRGs. The two-point correlation function at very small scales can be used to infer merger rates, assuming all LRG-LRG pairs closer than a given distance will eventually merge within a timescale given by the orbital or dynamical friction time. Masjedi et al. (2006) put an upper-limit on the LRG-LRG merger rate of $\approx 0.6 \times 10^4$ Gpc^4 Gyr^{-1}. This very low rate suggests that mergers between LRGs is not the primary cause of evolution in the population. In Masjedi et al. (2008) the authors extended this reasoning to other types of galaxies, by computing the cross-correlation between LRGs and both red and blue galaxies, of different luminosities. They found that most of the luminosity brought to LRGs comes from red galaxies via dry mergers and they put an upper limit on the growth of LRGs at 1.7 ± 0.1 h % Gyr^{-1} at $z \approx 0.25$. These upper limits sit of the low end of other measurements,

but it should be pointed out the Masjedi et al. (2006, 2008) measurements only take into account LRG growth that involves an already existent LRG - i.e., it fails to account for new LRGs being formed from the mutual merging of fainter (red) galaxies. Similarly, De Propris et al. (2010) looked at dynamically close pairs in the 2SLAQ sample (concentrating on pairs of galaxies in $0.45 < z < 0.65$), and found a merger rate of 0.6×10^4 Gpc^4 Gyr^{-1}, consistent with Masjedi et al. (2006) and reaching a similar conclusion.

Finally, one can look at the *evolution of the clustering* of the LRGs and ask whether it is consistent with passive-evolution. At its simplest, both White et al. (2007) and Wake et al. (2008) found *no evolution* in the clustering amplitude as a function of redshift. This alone is a significant problem for passive evolution, as a scale-independent and deterministic bias predicts evolution in the clustering strength. To go further, such analyses requires a framework for modeling this evolution. Conroy et al. (2007); White et al. (2007); Brown et al. (2008); Wake et al. (2008) have all, albeit in slightly different fashions, used the halo model to support their interpretation. Consistently, these studies find that, within the halo model framework, where there are too many satellites at low redshift if one is to assume passive evolution from the observed clustering at high-redshift (33 to 50 per-cent of the satellites must disappear). These galaxies must either merge with the central galaxy or be disrupted and become part of the intra-cluster light (ICL). Conroy et al. (2007) suggest that a significant amount of the stellar mass in the merged haloes never makes it to the central galaxy, and that this is a way to reconcile the observed lack of evolution in the mass or luminosity function of LRGs with clustering studies that indicate that a large number of mergers happened since z=1. This argument is given some strength by the fact that they can match the total stellar mass budget of clusters, and by the prediction of a significant amount of ICL around satellite galaxies that was seen in the Virgo cluster (Mihos et al. 2005).

Comparison between all of these studies is made very difficult by the different selection criteria, redshift range, and perhaps most importantly the number density of the sample, which in turn determines the luminosity/masses probed. Evolution of galaxies in the red sequence is heavily dependent on luminosity, with lower-luminosity galaxies suffering from significant evolution since z=1 (e.g. Brown et al. 2007).

1.1 This work

In this work we present an analysis of the evolution of LRGs in the complete sample of galaxies observed using the original SDSS LRG targeting algorithm (Eisenstein et al. 2001). We analyse the number and luminosity density of these galaxies, the evolution of the luminosity function, and clustering strength.

Our methodology significantly differs from previous works in two ways. Firstly, we introduce a new weighting scheme that allows us to match galaxies at low- and high-redshift whilst keeping most of the galaxies in the sample. Secondly, as part of our clustering analysis we analyse a luminosity-weighted power-spectrum and its evolution. On large-scales, this statistic is insensitive to the merging of galaxies within the sample assuming conservation of light, and provides information on the causes of evolution and the

population of galaxies affected. By comparing clustering for luminosity and number-density weighted samples, we bypass the need to introduce the halo model in order to analyse how evolution is occurring.

Throughout the paper, we use the Maraston et al. (2009) fiducial model for the expected colour evolution of an LRG, assuming passive evolution (M09). The *stellar* evolution is the only model dependence of this work, apart from dynamical passive evolution that we aim to test. Our choice of model is further discussed in Sections 2.1 and 6.

Our paper is organised as follows: in Section 2 we describe our samples, including selection, K+e-corrections, weighting-schemes and sample matching; in Section 3 we explain our method for the computation of the galaxy power-spectrum and in Section 4 its predicted evolution in the passive scenario; results are presented in Section 5; we explicitly consider uncertainties in the stellar model in Section 6; we consider the implications for the LRG population and present our interpretation in Section 7; a comparison with previous work is done in Section 8 and finally we summarize in Section 9.

2 THE LRG SAMPLE

We analyse the SDSS spectroscopic LRG sample, whose selection in colour and luminosity was described in Eisenstein et al. (2001). The upper panel of Fig. 1 shows the distribution of all of the galaxies in terms of colour. The red line shows the track predicted by the M09 model for a galaxy made up solely by stars that are 12 Gyr old at redshift of zero, and that have been left to passively evolve since. The lower panel of Fig. 1 shows the redshift distribution of the galaxies. In this paper we adopt the following nomenclature: SDSS model magnitudes are written as u, g, r, i, z; SDSS petrosian magnitudes as u_P, g_P, r_P, i_P, z_P and magnitudes given by the fiducial model of M09 as $u_m, g_m, r_m, r_m, i_m, z_m$.

The M09 model is used to match samples at low and high redshift, and in calculating rest-frame absolute magnitudes. The SDSS LRG selection, which was based on the PEGASE models (Fioc & Rocca-Volmerange 1999), is only important in that this defines the galaxies whose evolution we are testing. I.e. we can decouple the selection of the galaxies whose evolution we are testing with the model used to test that evolution. Essentially, in this paper, we test whether the SDSS LRGs selected using the Eisenstein et al. (2001) cuts are dynamically consistent with passive evolution, assuming a model for the colour evolution that we know is able to fit at least part of this sample (Maraston et al. 2009). One may also want to explore whether samples of galaxies that are further or closer to the fiducial model, in colour-colour space, follow passive evolution more or less closely. We leave that for a follow-up paper.

2.1 K+e corrections

We have used the observed colours and the fiducial model to compute the K- and K+e-corrections used throughout this paper. The M09 model is the only published model that matches the colour evolution of LRGs over our redshift range of interest, and therefore it is the only viable option for this
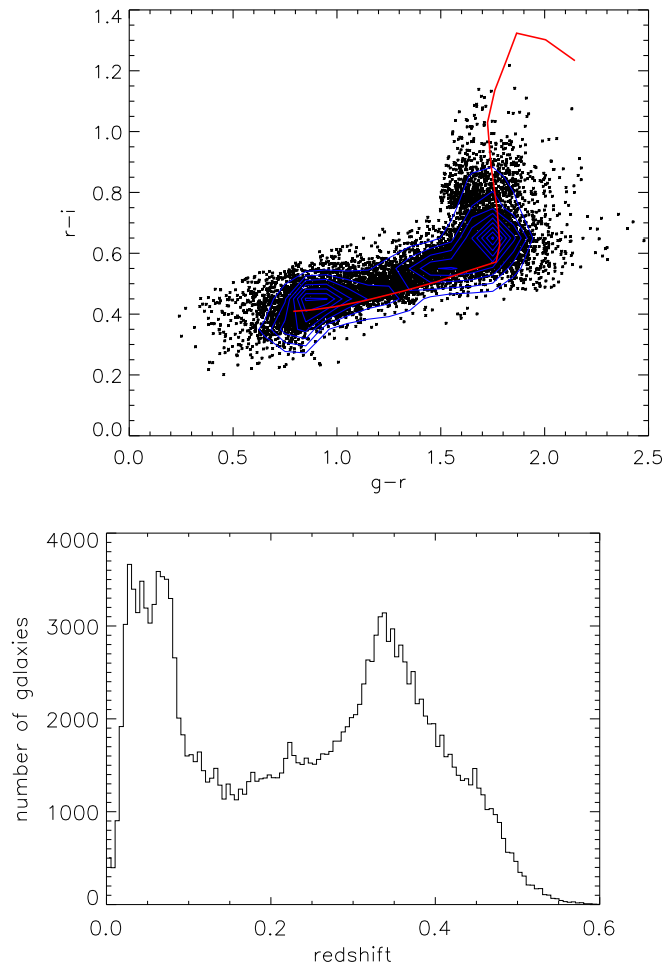
Figure 1. *Top:* Colour-colour plane for LRGs. The black points are a sub-set of 10,000 galaxies, and the blue contours are representative of the number density of points (as calculated from the full sample). The red line corresponds to the fiducial model of Maraston et al (2009). *Bottom:* Redshift distribution of the original sample. Below a redshift of 0.15 the LRG selection is heavily contaminated, and these galaxies are later discarded.

work. The solution offered in M09 stems from two major additions with respect to the previous literature: the inclusion of a sub-dominant metal-poor stellar component (as opposed to a young stellar component), and a change in the stellar library. Conroy & Gunn (2009) have raised some concerns about the latter because they, with their SPS method, could not replicate the changes reported in Maraston et al. (2009). This inconsistency will be considered further in Maraston et al. (2010, in prep). Additionally, in Maraston et al. (2009), the authors explicitly assume dynamical passive evolution of the data to which the model is fitted. If this assumption is relaxed one may well find that the inclusion of a metal-poor stellar component is no longer the only - or indeed the best - solution to the problem. The assumption of passive dynamical evolution, however, is the very hypothesis this paper aims to test, and therefore perfectly consistent with our analysis. Thus use of M09 models, which are the best fit to the ridge line of a sub-sample of SDSS selected LRGs, is consistent with the test we are performing.

The fiducial model provides $L_\lambda(t_{age})$, the luminosity per unit wavelength of an LRG of age t_{age}. To make our analysis more straightforward, we K+e-correct all galaxies to a common redshift of $z_c = 0.1$, and calculate corrected absolute magnitudes as

$$M_{r,0.1} = r_p - 5\log_{10}\left\{\frac{D_L(z_i)}{10\text{pc}}\right\} - Ke(z, 0.1), \qquad (1)$$

with

$$Ke(z, z_c) = \qquad\qquad\qquad\qquad\qquad\qquad (2)$$
$$= -2.5\log_{10}\left\{\frac{1}{1+z}\frac{\int T_{\lambda_o}L_{\lambda_o}(z)\lambda_o d\lambda_o \int T_{\lambda/(1+z_c)}\lambda_e^{-1}d\lambda_e}{\int T_{\lambda_o/(1+z_c)}L_{\lambda_e}(z_c)\lambda_e d\lambda_e \int T_{\lambda_o}\lambda_o^{-1}d\lambda_o}\right\}.$$

λ_o is in the observed frame and λ_e in the emitted frame. T_λ is the SDSS's r-band filter response, and $L_\lambda(z)$ the luminosity of a galaxy at redshift z, given the fiducial model. Traditionally, calculating K-corrected rest-frame magnitudes is done to the mean redshift of the sample, and is accompanied by a change in the filter's wavelength such that, for galaxies at that redshift (which should be the majority of the sample), the K-correction is independent of the galaxy's spectrum (often not known). However, note that Equation 2 gives a fixed K+e correction for a given redshift, and is independent of the actual observed colours or spectrum of each galaxy. The assumption is that the model is a good description of all galaxies in the sample. This makes the choice of the common redshift at which to normalise spectra, z_c, purely arbitrary.

A comparison of the rest-frame r-band K-corrected absolute magnitudes obtained using this model and the ones obtained using the code K-correct (Blanton & Roweis 2007) can be seen in Fig. 2. The scatter can be explained by the fact that K-correct does not use a fixed template, but rather fits a spectrum to the photometry in order to find the K-corrections. There is a small offset of around 0.03 magnitudes, which is roughly constant with magnitude, and the agreement is generally good.

2.2   Sample matching

In order to analyse the evolution of the LRG population, we construct a number of pairs of samples, with one sample in each pair at low and one at high redshift. The primary difficulty in doing this is selecting a sample at low-redshift that matches, in terms of individual galaxy properties, the evolved product of the sample at high-redshift. This sample-matching process has to take into account four redshift dependent effects:

(i) the intrinsic evolution of the colour and brightness of an LRG,
(ii) the varying errors on galaxy colour measurements,
(iii) the varying photometric errors in any one band.
(iv) the varying survey selection,

Our correction for (i) is unashamedly model-dependent. We work under the assumption that M09 is a good description of the colour evolution of the stellar populations, and assume passive dynamical evolution for the galaxies in our sample - the latter does not pose a problem for this work since it is the suitability of this model we are trying to investigate. We include an evolving colour scatter term to allow for (ii). This is described in Section 2.2.1.
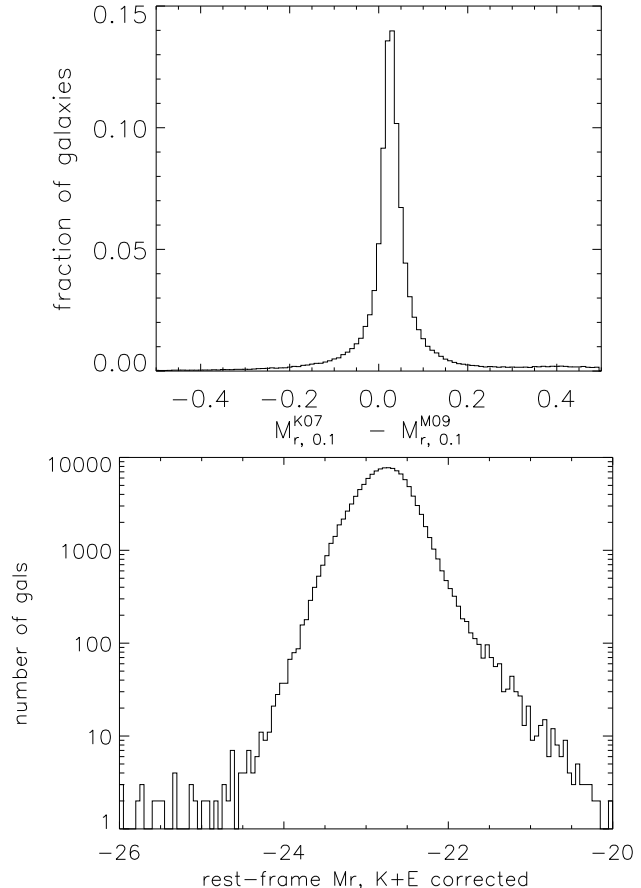

Figure 2. *Top:* The difference in k-corrected *only* rest-frame absolute magnitudes in the r-band when obtained with either k-correct (K07) or the M09 model. There is a small offset of around 0.03 magnitudes, which is roughly constant with magnitude. *Bottom:* Distribution of K+e corrected rest-frame magnitudes in the r-band for all galaxies at $z > 0.15$.

We show that (iii) is a negligible effect in Section 2.3 by creating mock samples.

Traditionally (iv) has been satisfied by removing galaxies that could not have been observed in the other sample in the pair (Wake et al. 2006, 2008). However this is wasteful in that, in order to fully match samples including distributions within each, we need to remove galaxies that could not have been observed across all of both samples. In contrast, our approach for (iv) is to construct a set of weights that assures that each population of galaxies - in terms of colour and absolute magnitude - is given the same weight in the high and low redshift samples. For a catalogue whose selection is only based on a magnitude limit, the traditional V_{max} estimator could be used for this instead. We explain our weighting scheme in Section 2.2.3, which differs in that it is designed to be optimal in the limit of Poisson errors.

2.2.1   Predicting LRG colours and magnitudes with redshift

In order to match samples, we need to predict the colour and magnitude that an observed LRG would have if it was moved to a range of redshifts following passive evolution.
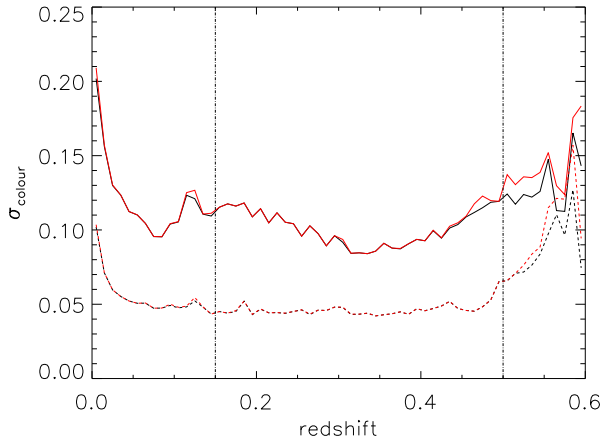
Figure 3. σ_{g-r} (solid line) and σ_{r-i} (dashed line), calculated with respect to the fiducial model of Maraston et al (2009), as a function of redshift. The red lines are the standard deviations obtained after correcting for the fact that we are only sampling a finite range in colour and are the ones we use in this work. The vertical lines represent the redshift range used.

This will depend on i) the observed colours and absolute magnitude; ii) the fiducial evolutionary model. In order to match observed samples we also need to account for the evolution of the colour-colour scatter that has a clear redshift dependence.

We are assuming a single evolutionary model, so for any given redshift the predicted colours are fixed. To calculate the colours of an LRG at any redshift, we must include some sort of departure from the fiducial model that takes into account the observed scatter.

We start by calculating the scatter with respect to the model, as a function of redshift, for each of the two colours. This can be seen in Fig. 3, where we show $\sigma_{g-r}(z)$ and $\sigma_{r-i}(z)$. Due to target-selection cuts in the colour-colour plane, we are not guaranteed to fully sample the distribution of $g-r$ and $r-i$, which may affect our estimate of $\sigma_{g-r}(z)$ and $\sigma_{r-i}(z)$. We are in the regime where this effect is small and we assume that the estimation of the mean is unbiased. We therefore apply a correction to σ given by

$$\Delta\sigma^2 = \int_{-\infty}^{a}(x-\langle x\rangle)^2 p(x)dx + \int_{b}^{-\infty}(x-\langle x\rangle)^2 p(x)dx \quad (3)$$

where a and b represent the limits sampled by the data, and $p(x)$ is the probability distribution which we assume to be Gaussian. In practice we estimate a and b from the data at each redshift (finding that $|a,b| \gg \sigma$), and use the uncorrected value of σ to estimate $p(x)$ and evaluate the integral. Fig. 3 shows that the correction is small within the redshift range probed.

Having calculated the scatter, we require that the colour at a redshift z' of a galaxy observed at z_0 departs from the fiducial model in a way such that the ratio of the distance from the data point to the model, $\Delta(g-r)$, and the scatter at that z_0 is maintained at any other redshift. Explicitly:

$$(g-r)(z')=(g-r)_m(z')+\Delta(g-r)(z_0)\frac{\sigma_{g-r}(z')}{\sigma_{g-r}(z_0)}, \quad (4)$$

and similarly for $r-i$. Note that we are assuming that the observed scatter in colour is mostly intrinsic or due to pho-
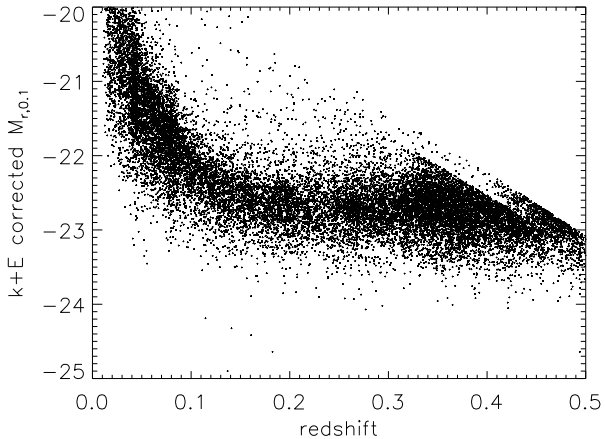
Figure 4. K+e corrected absolute magnitude as a function of redshift.

tometric errors. I.e., that both cuts are wide enough that they sample the LRG population almost completely. This is not strictly true, but we find that it is indeed almost exactly true, as can be seen by the corrections applied to σ_{g-r} and σ_{r-i} in Fig. 3.

We calculate petrosian r-band magnitudes and surface brightness as a function of redshift as

$$r_p(z') = M_{r,0.1} + 5\log_{10}\left\{\frac{D_L(z')}{10pc}\right\} + \mathrm{Ke}(z',0.1) \quad (5)$$

$$\mu_{50}(z') = r_P(z') + 2.5\log_{10}[2\pi\theta_{50}^2(z')]. \quad (6)$$

The K+e-corrections are given by Equation 2. Equation 6 assumes that the physical size of a galaxy does not change with redshift, and $\theta_{50}(z') = \theta_{50}(z_0)\frac{D_A(z_0)}{D_A(z')}$ with D_A being the angular diameter distance.

Note that as it is written, the predicted evolution of $r_p(z)$ does not take into account the changing photometric error with redshift. The observed scatter in $r_p(z)$ is due both to the increase in the photometric errors and the scatter in intrinsic luminosity. It is hard to disentangle the two on a galaxy by galaxy basis, so instead we test the effect of assuming a constant error with redshift on our sample matching and selection methodologies. The effect is found to be negligible, and we give more details in Section 2.3.

This gives us the colours, petrosian magnitude and surface brightness as a function of redshift, which allows us to know where each galaxy would be observed within the survey. Recall that for each galaxy we also have a redshift, and a K+e corrected $r^{0.1}$-band rest-frame absolute magnitude. The redshift - absolute magnitude plane can be seen in Fig. 4. This figure clearly shows that the SDSS colour cuts result in a sample that doesn't easily lend itself to a volume-limited analysis. The two sharp diagonal edges correspond to the two r_P-band limits in cut I and cut II at $r_P < 19.2$ and $r_P < 19.5$ respectively.

2.2.2 Photometric errors

As mentioned in Section 2.2.1, there is an added subtlety in this selection that comes from the fact that photometric errors increase with redshift. We do not model this in r_p when we construct and match our samples. That puts us in a

potentially vulnerable position with respect to a Malmquist type of bias, in which a slope in the number density with luminosity may result in more faint objects being scattered into a sample than bright objects are scattered out. Note that if the error was constant with redshift our weighting scheme would perfectly correct for that because we match the weight of each population at high and low redshift, for any given magnitude cut - so we would match any excess or deficit of objects.

To check the effect of assuming a constant error we do the following. We estimate the true luminosity function of LRGs by using a V_{max} weight on our full catalogue, and use it to construct high and low-redshift mock catalogues in the magnitude ranges that we adopt for our final catalogues (see Section 2.3). We do this twice for each catalogue: once accounting for the changing error with redshift in r_p, and once assuming a constant error. The effect in the number and luminosity density in each catalogue between the two methods is between 0.05% and 0.3%, depending on the magnitude cuts. The effect is small enough that we ignore it for the rest of this paper.
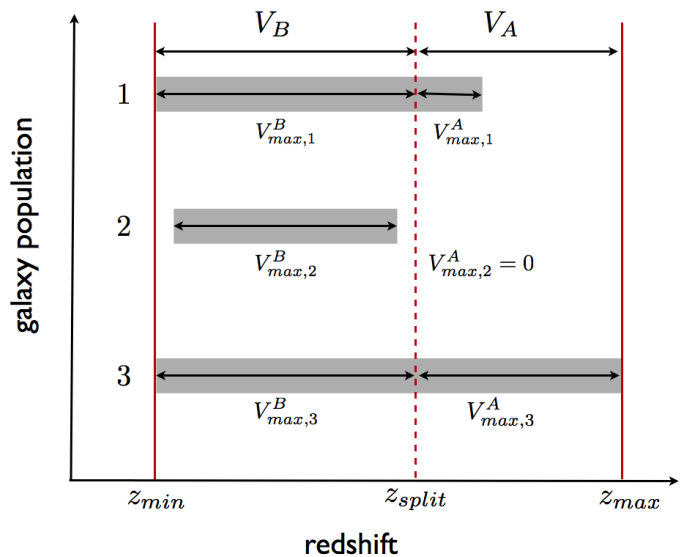
2.2.3   Weighting scheme

In this paper we only consider two redshifts slices, which occupy a volume V_A (at high-redshift) or V_B (at low-redshift). Using the analysis described above, we can calculate the maximum volume within each redshift slice that a galaxy could have been observed in, given its measured colours and redshift. A traditional V_{max} correction to match the samples at high and low redshift would use this information to up-weight galaxies by the reciprocal of the fraction of the volume of the respective redshift slice within which a galaxy could be observed. i.e. we should apply a weight to each galaxy

$$w_i = \frac{V_{\mathrm{slice}}}{V_{\mathrm{max},i}}, \qquad (7)$$

where $V_{max,i}$ is the volume the galaxy could have been observed in a redshift slice, given the evolution of its optical properties and the characteristics of the colour cuts, and V_{slice} is the total volume of the redshift slice the galaxy falls in. Galaxies that can be observed across all of the slice in which they fall are given a weight of unity, but galaxies that could only have been observed in part of the slice are given a larger weight, to compensate for identical galaxies that exist at other redshifts but fail to meet the survey selection criteria. Such a weighting scheme fails to remove any galaxies that are not seen *at all* in the other redshift slice, leaving the match between the two slices unbalanced in terms of galaxy properties. Furthermore, we also risk massively up-weighting populations that only exist in very small numbers in a slice, and Poisson errors of such galaxies may dominate.

Instead, we construct a new scheme that keeps the total weight of each galaxy population the same in the different redshift slices by *down-weighting* galaxies based the minimum fractional volume that the galaxy could have been observed in for both slices. Explicitly, for a galaxy in V_A we calculate

$$w_i = \frac{V_A}{V_{\mathrm{max},i}^A} \min\left\{ \frac{V_{\mathrm{max},i}^A}{V_A}, \frac{V_{\mathrm{max},i}^B}{V_B} \right\}, \qquad (8)$$

Figure 5. A schematic representation of our weighting scheme, given by Equations 8 and 9. We give three different examples. In each case, the grey stripe represents the volume a given type of galaxy could be observed in (see main text for details).

and similarly for a galaxy in V_B:

$$w_i = \frac{V_B}{V_{\mathrm{max},i}^B} \min\left\{ \frac{V_{\mathrm{max},i}^A}{V_A}, \frac{V_{\mathrm{max},i}^B}{V_B} \right\}. \qquad (9)$$

Where the traditional V_{max} estimator would up-weight galaxies, we instead down-weight the corresponding galaxies with the same properties in the other slice.

In Fig. 5 we schematically show three representative populations of galaxies. Here population refers to a set of galaxies that have similar colours and luminosities. A galaxy in population 1 that is observed in V_A, for example, is given a weight of unity, according to equation 8. A traditional V_{max} weight would up-weight this galaxy by $V_A/V_{max,1}^A$, but our approach instead down-weights the population 1 galaxies seen in V_B. This automatically takes care of problematic situations like population 2, which is constrained to one of the redshift slices - in this case it would be given a weight of zero. Population 3 simply represents the galaxies that we can see everywhere in the survey - in this case the weight is always unity meaning we are of course volume-limited for this particular population. The weighting is done on a galaxy-by-galaxy basis.

We have to be careful in the interpretation of results where we use our weighting, compared with the traditional V_{max} weighting. Whereas the latter gives us the means to correct for incompleteness and yields true space densities, the former should be thought as a weighting scheme rather than a completeness correction. This means that weighted number and luminosity densities calculated in this way *are still potentially volume incomplete*, but the populations are weighted in such a way that they are equally represented at both redshifts. We can compare the distribution of total weighted luminosity for the two slices, but we cannot interpret these functions as giving the luminosity density.

The advantage of this weighting scheme over simply matching samples by removing galaxies that do not match

the selection criteria in the other slice is that we keep a large proportion of the sample - in fact, the number of galaxies thrown out due to the situation of population 2 in Fig. 5 is very small. These galaxies contain no information about galaxy evolution between the two samples as galaxies of that type (luminosity, colour) only exist in one of the samples. Consequently, no information is lost by removing these galaxies. It is easy to see that the remaining galaxies are weighted optimally in terms of Poisson statistics: the importance of each sub-population is dependent on the smallest number of galaxies of that type in either sample, and is given a weight accordingly. We present the final size of our samples, after applying the sample selection method described in the next Section, in Table 2.3.

2.3 Sample selection

In the rest of this paper we consider only the galaxies with redshifts in $[0.15, 0.5]$. We start by selecting galaxies that are brighter than a given chosen absolute K+e corrected magnitude, $M_{r,0.1}^{lim}$, which can be varied. The sample is split at the median redshift, to ensure that we have the same number of objects in each slice to begin with. As in Section 2.2.3, we have labelled the high-redshift sample as sample A, occupying a volume V_A and the low-redshift sample as sample B, over a volume V_B.

We then calculate the integrated *weighted* luminosity of the sample as

$$I_A \equiv \int_{L_{min,A}}^{\infty} N(L)LdL = \sum_{L_i > L_{min,A}} L_i w_i, \qquad (10)$$

where $N(L)dL$ is the number of LRGs with luminosity in $[L, L + dL]$. In practice we simply use $L = 10^{-M_r/2.5}$ as a proxy for luminosity, which is essentially a luminosity in arbitrary units and $L_{min,A} = 10^{-M_{r,0.i}^{lim,A}/2.5}$. $M_{r,0.i}^{lim,A}$ is arbitrarily chosen and can be varied so that we may learn about the evolution of LRGs as a function of magnitude. We can the compute a weighted luminosity density as

$$\ell_A = \frac{I_A}{V_A}. \qquad (11)$$

This is the luminosity density expected in the $r^{0.1}$-band, at $z = 0.1$, from LRGs in the high-redshift slice, weighted to match the galaxies observed at low redshift. Alternatively and in an identical fashion, we can also calculate the weighted number density of the sample as

$$N_A \equiv \int_{L_{min,A}}^{\infty} N(L)dL = \sum_{L_i > L_{min,A}} w_i, \qquad (12)$$

and define a total weighted number density as

$$n_A = \frac{N_A}{V_A}. \qquad (13)$$

We now wish to construct a sample at low redshift that matches either the luminosity or number density of the sample at high redshift. To do this we find $L_{min,B}$ such that

$$\ell_B \equiv \frac{1}{V_B} \int_{L_{min,B}}^{\infty} N(L)LdL = \frac{1}{V_B} \sum_{L_i > L_{min,B}} L_i w_i = \ell_A, \qquad (14)$$

or, alternatively,

$$n_B \equiv \frac{1}{V_B} \int_{L_{min,B}}^{\infty} N(L)dL = \frac{1}{V_B} \sum_{L_i > L_{min,B}} w_i = n_A. \qquad (15)$$

We can always associate a $M_{r,0.1}^{lim,B}$ with $L_{min,B}$, but note that it will be different from $M_{r,0.1}^{lim,A}$, even for samples matched by luminosity-density. This on itself is a potential estimator of how much a sample deviates from passive evolution. However, in this paper we will instead concentrate on *weighted* number and luminosity densities alone - a comparison between the luminosity-density obtained when matching on number-density and vice-versa may immediately tell us if the data does not support with passive evolution, we look at this in Section 5.1. For the rest of this paper, when we consider the limiting magnitude of the sample we are referring to the magnitude cut at high-redshift. For reference, we give $M_{r,0.1}^{lim,A}$ and $M_{r,0.1}^{lim,B}$ for each of our samples in Table 2.3.

2.3.1 Choice of z_A and z_B

The entirety of this work is based on comparing two redshift slices. However, *both* the boundary between these two slices and the redshift distributions within each slice depend heavily on the faint magnitude chosen. As we include fainter galaxies, we predominantly enrich the sample with low-redshift galaxies, producing a gradient of galaxy density across each sample that will depend on the magnitude limit of that sample. The picture is further complicated as we weight galaxies as described in Section 2.2.3. We must therefore consider weighted redshift distributions, and use the mean of these weighted distributions to give a representative redshift for each slice. Explicitly,

$$\bar{z}_A = \frac{\sum_{z_i \in V_A} z_i w_i}{\sum_{z_i \in V_A} w_i}, \qquad (16)$$

and similarly for $\bar{z}_B$. The values for $\bar{z}_A$, $\bar{z}_B$ and the boundary, z_{split} are given in Table 2.3.

3 MEASURING THE CLUSTERING

Power-spectra for the galaxy samples were calculated using the method described by Feldman et al. (1994). Each galaxy distribution is converted to an over-density field by placing the galaxies on a grid and subtracting an unclustered "random catalogue", which matches the galaxy selection. To calculate this random catalogue, we model the redshift distribution of the galaxies using a spline model (Press et al. 1992), and model the angular mask using a routine based on a HEALPIX (Górski et al. 2005) equal-area pixelization of the sphere as in Percival et al. (2009).

Each galaxy and random is weighted using the method described in Section 2.2.3. In order to assign luminosities to the randoms, we randomly draw a luminosity from the galaxy catalogue, with the constraint that the redshift of the data point lies within 0.02 of the redshift of the new random point. The weight of the same galaxy is assigned to the random point - this ensures that the redshift distributions of the V_{max}-weighted samples are the same for the data and random catalogues. For simplicity, we do not include a

| | $M_{r,0.1}^{lim,A}$ | $\bar{z}_A$ | $\bar{z}_B$ | z_{split} | $M_{r,0.1}^{lim,B}$ | Sample size | |
						V_A	V_B
n-matched	-23	0.44	0.29	0.38	-23.04	12,998	11,938
ℓ-matched		0.44	0.29	0.38	-23.04	12,998	11,615
n-matched	-23.9	0.43	0.28	0.37	-22.95	19,567	16,226
ℓ-matched		0.43	0.28	0.37	-22.96	19,567	15,650
n-matched	-23.8	0.43	0.28	0.36	-22.89	27,328	19,433
ℓ-matched		0.43	0.28	0.36	-22.90	27,328	18,300
n-matched	-22.7	0.42	0.27	0.35	-22.81	35,632	23,654
ℓ-matched		0.42	0.27	0.35	-22.83	35,632	22,135
n-matched	-22.6	0.41	0.26	0.34	-22.75	43,828	27,269
ℓ-matched		0.41	0.26	0.34	-22.77	43,828	25,209
n-matched	-22.5	0.40	0.26	0.33	-22.70	50,994	29,384
ℓ-matched		0.40	0.26	0.33	-22.73	50,994	26,677
n-matched	-22.4	0.40	0.26	0.33	-22.68	56,632	29,687
ℓ-matched		0.40	0.26	0.33	-22.72	56,632	26,155
n-matched	-22.3	0.39	0.25	0.32	-22.65	60,828	30,855
ℓ-matched		0.39	0.25	0.32	-22.70	60,828	26,915

Table 1. Basic parameters for the LRG samples analysed in this paper.

luminosity-dependent bias model that normalizes the fluctuations to the amplitude of L_* galaxies as advocated by Percival et al. (2004).

Inclusion of the standard Feldman et al. (1994) weight

$$w_i^n = \frac{1}{1 + \bar{n}_i \bar{P}}, \quad (17)$$

would potentially change the match between the high-z and low-z samples, because the distribution of galaxy number densities in each slice will be correlated with galaxy properties, and the correlation may be different for the high-z and low-z samples. We therefore do not include this weight. Given that the number density of the total SDSS LRG population is approximately constant with redshift, this only has a small impact on the error with which we can measure the galaxy clustering strength.

Power spectra were calculated using a 1024^3 grid in a series of cubic boxes. A box of length $4000\,h^{-1}$ Mpc was used initially, but we then sequentially divide the box length in half and apply periodic boundary conditions to map galaxies that lie outside the box. For each box and power spectrum calculation, we include modes that lie between $1/4$ and $1/2$ the Nyquist frequency (similar to the method described by Cole et al. 2005), and correct for the smoothing effect of the cloud-in-cell assignment used to locate galaxies on the grid (e.g. Hockney & Eastwood 1981, chap. 5). The power spectrum is then spherically averaged, leaving an estimate of the "redshift-space" power. This method is the same as that used in Percival et al. (2009); Reid et al. (2009).

In order to interpret the evolution in the power spectra measured between high-z and low-z samples, we need to know the effect of the survey geometry on the recovered power. This window function can be expressed as a matrix relating the true power spectrum evaluated at wavenumbers k_n, $P_{true}(k_n)$, to the observed power spectrum $P_{obs,i}$, where i refers to the different band-powers with central wavenumbers k_i:

$$P_{obs,i} = \sum_n W(k_i, k_n) P_{true}(k_n) - W(k_i, 0). \quad (18)$$

The term $W(k_i, 0)$ arises because we estimate the average

galaxy density from the sample, and is related to the integral constraint in the correlation function (Percival et al. 2007). The window function allows for the mode-coupling induced by the survey geometry. Window functions for the measured power spectrum (Eqn. 15 of Percival et al. 2004) were calculated as described in Percival et al. (2001), Cole et al. (2005), and Percival et al. (2007).

The covariance matrices for the measured power spectrum band-powers (including correlations between the power spectra from the different redshift slices), were calculated from 10^4 Log-Normal (LN) catalogues (Coles & Jones 1991; Cole et al. 2005). Catalogues were calculated on a $(512)^3$ grid with box length $4000\,h^{-1}$ Mpc as in Percival et al. (2009), where LN catalogues were similarly used to estimate covariance matrices. Unlike N-body simulations, these mock catalogues do not model the growth of structure, but instead return a density field with a log-normal distribution, similar to that seen in the real data. The window functions for these catalogues were matched to that of the halo catalogue. The input power spectrum was a ΛCDM model matched to the large-scale shape of the observed power spectra.

After removing the effect of the window, we simultaneously fitted the amplitude of the low- and high-redshift power-spectra amplitudes using the full covariance matrix. We are interested in the large scales only - small scales will be affected by intra-halo terms and are sensitive to merging happening at these scales. The results presented in Section 5.3 are amplitudes fitted only up to $k_{max} = 0.15$. Our results are robust to changing this scale cut-off within the range $k_{max} \approx 0.1 - 0.2$. Even though we use the full covariance matrix when fitting the amplitudes (which takes into account correlations between the two redshift slices), we find that the power-spectra are almost independent across the two slices. The 1-sigma errors shown in Section 5.3 are therefore simply calculated assuming this is strictly true.

The Feldman et al. (1994) methodology assumes that galaxies form a Poisson sampling of a Gaussian random field. The resulting shot noise, which arises because of this sampling, is traditionally subtracted from the measured power spectra. Weighting galaxy populations at different redshifts

by luminosity means that the large-scale clustering strength is expected to be unchanged by loss-less mergers. However, the predicted shot-noise would be changed by galaxy mergers: for example, the expected shot-noise from two equal-weight galaxies, or one galaxy with twice the weight, are different. Consequently, for our luminosity weighted samples, we consider a scenario where we fit both the large-scale amplitude and the shot-noise, in addition to subtracting the standard Poisson shot-noise.

4   PREDICTING THE CLUSTERING AMPLITUDE

The observed evolution in the large-scale galaxy power-spectrum is the combination of the growth of the fluctuations in the underlying density field, parametrized by the linear growth factor $D(z)$, and the evolution of galaxy bias set by the peculiar velocity field. We assume that the expected evolution of the amplitude of the redshift-space power spectrum between the two redshift slices is given by (Kaiser 1987)

$$P_g(k, z_B) = \frac{b_B^2 + \frac{2}{3}b_B f_B + \frac{1}{5}f_B^2}{b_A^2 + \frac{2}{3}b_A f_A + \frac{1}{5}f_A^2} \frac{D_B^2}{D_A^2} P_g(k, z_A). \quad (19)$$

Here f is the standard logarithmic derivative of the linear growth factor with respect to the logarithm of the scale factor. For simplicity, we take $f \simeq \Omega_m^{\gamma(z)}$, $\Omega_m = 0.25$ with $\gamma(z) \simeq 0.557 - 0.02z$, which is accurate to 0.3% for this cosmological model (Polarski & Gannouji 2008).

For a passively evolving population, we assume that the evolution in the bias is given by Fry (1996)

$$b_z = (b_0 - 1)/D_z + 1, \quad (20)$$

where b_0 is the bias at zero redshift. In practice, we compute b_A from the data, and calculate

$$b_B = \frac{(b_A - 1)D_A}{D_B} + 1. \quad (21)$$

It is worth noting that the Fry (1996) model assumes that the distribution of galaxy velocities matches that of the mass. Simulations show that this is reasonable for the haloes in which LRGs are expected to reside (White et al. 2007), although it is possible to create models, albeit ones that are somewhat contrived, in which this would not hold, such as placing LRGs at stationary points in the density field.

To calculate the growth factor we use the fitting formulae of Carroll et al. (1992) to calculate the correction to the growth factor from an Einstein-de Sitter to a ΛCDM model.

Fig. 6 shows the expected evolution in the bias, growth factor, and overall power-spectrum amplitude for the redshift ranges we explore in this paper.

5   RESULTS

We now present results based on using our high and low redshift samples to perform the tests of passive evolution described in Section 1 on the number and luminosity densities, the luminosity function, and the clustering strength.

5.1   Number and luminosity densities

Matching samples based on total numbers of galaxies, obviously allows us to test how the number density changes between the redshift slices. If some proportion of the galaxies seen in the high redshift sample are expected to merge before present day, then the merger products will be included in the low-redshift sample. In this situation, matching number density between samples will bring *extra* galaxies into the low-redshift sample. We should also find that the total luminosity changes between the samples if no light is lost to the intra-cluster medium through the mergers. Under the same assumption, matching samples based on total luminosity will not bring in these extra galaxies, although we will see a reduction in the total number of galaxies. Table 2 shows our results for a variety of magnitude ranges; all ratios are of z_A/z_B.

Fig. 7 presents the values in bold in Table 2 and shows how the change in number and luminosity density changes as a function absolute magnitude. The behaviour seen is perfectly consistent with a scenario where a small proportion of the LRGs within the sample at high-redshift merge to give brighter LRGs at low-redshift - we see a decrease in the number density for luminosity-matched samples and an increase in the luminosity density for number-density matched samples. This is not, however, the only explanation. Merging could have also happened between galaxies outwith the the sample - i.e., galaxies *fainter* than the magnitude cut merging into brighter galaxies between the two redshifts. As we will see later, our clustering analysis will help us distinguish between these two scenarios.

It is worth pointing out that the interpretation of Fig. 7 and Table 2 is not straight-forward because the redshift slices change as a function of magnitude. As we include fainter galaxies in the sample, these are predominantly at low redshift, and alter the median value that is used to split the sample. The effect measured is probably a combination of the inclusion of fainter galaxies and the fact that the split occurs at lower redshift - the latter is a small effect, but both can act to increase the number of mergers.

To make the interpretation easier, we can translate the ratio of galaxy number density into a percentage number of mergers per Gyr^{-1}, following the assumption that differences in number density are caused by loss-less mergers. This only makes sense in our luminosity-matched samples, where the low-redshift sample does not contain extra galaxies. We take the effective time interval Δt as being that between $\bar{z}_A$ and $\bar{z}_B$, and calculate

$$r_N(M < M_{r,0.1}) = \left(1 - \frac{n_B}{n_A}\right)\frac{1}{\Delta t}, \quad (22)$$

where n_A and n_B are weighted number densities as defined in (12) and (13). We show this rate, as a percentage and as a function of magnitude as the solid line in Fig. 8; the error bars are Poisson errors. Clearly, interpreting this plot as a merger rate only makes sense if one assumes that LRG-LRG mergers (from within each sample) are the cause to the change in the number density. If instead we have fainter galaxies merging together to enter the sample then the change in numbers can only be interpreted as a more general growth rate.

We can also do a similar analysis for the fractional luminosity growth for samples that have been matched to have
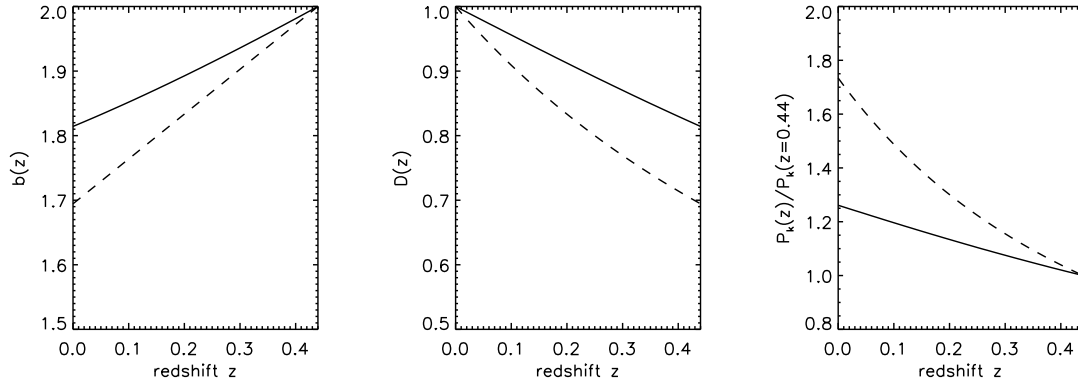
Figure 6. The evolution of the bias (left), growth factor (middle) and power-spectrum large-scale amplitude (right) for a population of passively evolving galaxies. The dashed line assumes an Einstein de-Sitter model, and the solid line includes a correction for ΛCDM.

| | | *n*-matched, V_{match} | | *n*-matched, V_{max} | | ℓ-matched, V_{match} | | ℓ-matched, V_{max} | |
		n	ℓ	n	ℓ	n	ℓ	n	ℓ
	z_A	4.56e-06	8886	4.98e-06	9705	4.56e-06	8886	4.98e-06	9705
$M_{r,0.1} < -23.0$	z_B	4.56e-06	9082	4.76e-06	9522	4.43e-06	8885	4.63e-06	9308
	Ratio	-	**0.978±0.0109**	-	-	**1.026±0.0133**	-	-	-
	z_A	6.44e-06	11761	7.52e-06	13553	6.44e-06	11761	7.52e-06	13553
$M_{r,0.1} < -22.9$	z_B	6.44e-06	12069	6.97e-06	13016	6.24e-06	11761	6.72e-06	12634
	Ratio	-	**0.974±0.00949**	-	-	**1.032±0.0114**	-	-	-
	z_A	8.38e-06	14426	1.05e-05	17644	8.38e-06	14426	1.05e-05	17644
$M_{r,0.1} < -22.8$	z_B	8.38e-06	15023	9.36e-06	16626	7.97e-06	14426	8.80e-06	15822
	Ratio	-	**0.960±0.00888**	-	-	**1.052±0.0105**	-	-	-
	z_A	1.04e-05	17080	1.42e-05	22423	1.04e-05	17080	1.42e-05	22423
$M_{r,0.1} < -22.7$	z_B	1.04e-05	17770	1.24e-05	20724	9.89e-06	17080	1.156e-05	19626
	Ratio	-	**0.961±0.00588**	-	-	**1.052±0.00826**	-	-	-
	z_A	1.22e-05	19253	1.83e-05	27287	1.22e-05	19253	1.83e-05	27286
$M_{r,0.1} < -22.6$	z_B	1.22e-05	20102	1.54e-05	24579	1.16e-05	19253	1.42e-05	23033
	Ratio	-	**0.958±0.00566**	-	-	**1.058±0.00790**	-	-	-
	z_A	1.38e-05	20975	2.23e-05	31534	1.38e-05	20975	2.23e-05	31534
$M_{r,0.1} < -22.5$	z_B	1.378e-05	22105	1.78e-05	27669	1.28e-05	20975	1.61e-05	25554
	Ratio	-	**0.949±0.00557**	-	-	**1.072±0.00783**	-	-	-
	z_A	1.48e-05	21983	2.54e-05	34543	1.48e-05	21983	2.54e-05	34543
$M_{r,0.1} < -22.4$	z_B	1.48e-05	23523	1.949e-05	29673	1.36e-05	21983	1.70e-05	26757
	Ratio	-	**0.934±0.00557**	-	-	**1.094±0.00801**	-	-	-
	z_A	1.57e-05	22811	2.81e-05	37014	1.57e-05	22811	2.81e-05	370134
$M_{r,0.1} < -22.3$	z_B	1.57e-05	24478	2.10e-05	31501	1.42e-05	22811	1.81e-05	28113
	Ratio	-	**0.932±0.00552**	-	-	**1.099±0.00798**	-	-	-

Table 2. The number and luminosity densities of high (z_A) and low (z_B) redshift samples for a range of magnitude cuts, for different matching schemes and using different weights. The values shown for a V_{max} weight are given only for reference, and all results are based on the V_{match} weights. Magnitudes are K+e corrected to $z = 0.1$; number densities are in units of Mpc^{-3} and luminosity densities are in arbitrary units. Note that z_A and z_B are not necessarily the same for the different magnitude cuts. A plot of the ratios in bold in these table is shown in Fig. 7.

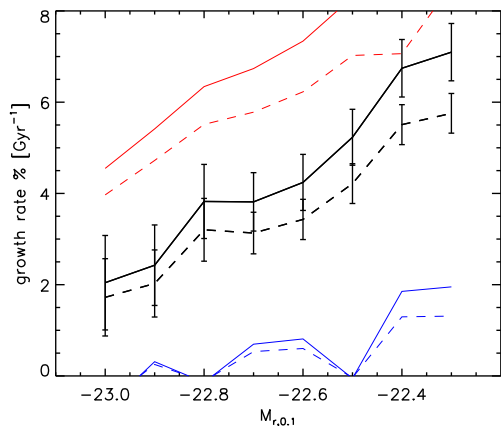the same number density. In this case, we compute

$$r_\ell(M < M_{r,0.1}) = \left(\frac{\ell_B}{\ell_A} - 1\right)\frac{1}{\Delta t}, \qquad (23)$$

where ℓ_A and ℓ_B are weighted luminosity densities as defined in (10) and (11). We show this fractional growth rate as the

dashed line in Fig. 8. This gain in luminosity to low redshift, depends on the new galaxies brought into the low-redshift sample, and cannot therefore be as easily interpreted by a merger model as the luminosity-matched samples. We quote the values of r_N and r_ℓ, including Poisson error bars, in Table 3.
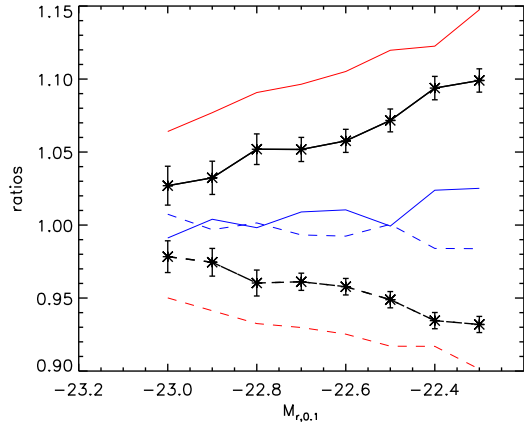
Figure 7. The ratio of the number density at high and low redshift when matching using the luminosity density (black solid line) and the ratio of the luminosity density at high and low redshift when matching using the number density (black dashed line). This plot shows the values in bold in Table 2. The blue and red lines show the estimated effect of uncertainties in the IMF slope (see Section 6 for details)
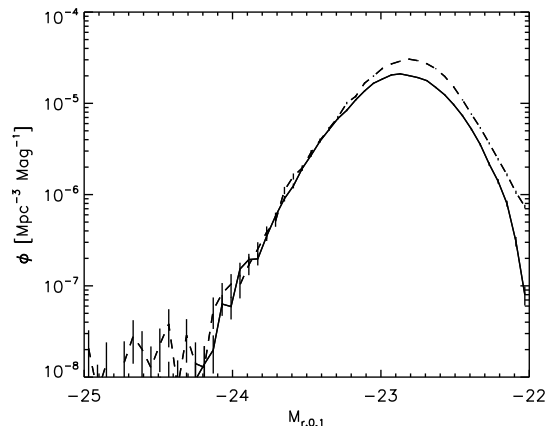
$M_{r,0.1}^{lim,A}$	$r_N \times 100$	$r_\ell \times 100$
-23.0	2.04 $\pm$1.035	1.72 $\pm$0.847
-22.9	2.43 $\pm$0.883	2.02 $\pm$0.735
-22.8	3.82 $\pm$0.812	3.20 $\pm$0.689
-22.7	3.81 $\pm$0.640	3.13 $\pm$0.455
-22.6	4.24 $\pm$0.614	3.43 $\pm$0.441
-22.5	5.23 $\pm$0.612	4.21 $\pm$0.436
-22.4	6.74 $\pm$0.630	5.51$\pm$0.438
-22.3	7.10 $\pm$0.628	5.75 $\pm$0.435

Table 3. The measured values of r_N and r_ℓ, as defined by equations (22) and (23) and plotted in Fig.8.

Figure 9. The luminosity function in V_A (solid line) and V_B (dashed line), as defined by Equation 24. The redshift boundary between the two volumes is $z = 0.33$. Given our V_{match} weighting scheme, this luminosity function is not corrected for volume completeness. Instead, it is constructed such that the population at low redshift is perfectly matched to the population at high redshift, see text for details.

Figure 8. The solid black line shows $r_N \times 100$: the percentile growth rate in number of galaxies per Gyr, as defined by equation 22. This can be interpreted as a merger rate if we assume that galaxies in the sample at high redshift have merged. The dashed black line shows $r_\ell \times 100$: the percentile increase in luminosity density for samples matched to have the same number density, as defined by equation 23. Both quantities are shows as a function of the faint magnitude limit, and given in Table 3. The blue and red lines show the estimated effect of uncertainties in the IMF slope (see Section 6 for details).

5.2 Luminosity function

The next natural step is to construct a luminosity function and study its evolution, which we compute for each of redshift slices as

$$\phi(M_{r,0.1})\Delta M_{r,0.1} = \sum_{M_i \in \Delta M_{r,0.1}} \frac{w_i}{V_{slice}}. \quad (24)$$

This does not give a luminosity function in the traditional sense, but rather it gives a population-weighted luminosity function. I.e., the luminosity function of galaxy samples at two redshifts that represent the same population of galaxies in equal terms, albeit perhaps incompletely. We show this pseudo-luminosity function in Fig. 9.

Fig. 9 shows that the information content is not significantly improved from that in Figs. 7 & 8, which show the change in the full sample. This is simple to understand: small differences in number density are always diluted when one splits them into magnitude bins. Fig. 9 does make it clear that one needs a way to enrich the low-redshift sample with galaxies of $M_{r,0.1} > -23$, by means other than passive stellar evolution.

5.3 Clustering

The last test that we perform is based on measuring the evolution of the clustering of our matched samples of LRGs. The

V_{match} -weighting makes sure that we are comparing like-with-like galaxies for clustering measurements. Matching the total luminosity means that, even allowing for loss-less mergers, we are comparing galaxies at low-redshift that are evolved products of the high-redshift galaxies without bringing extra galaxies into the sample. Additionally, weighting by evolved luminosity, means that the large-scale clustering should not be affected by these mergers: on large-scales there is no change in the clustering strength if two galaxies merge. The method for power spectrum measurement was described in Section 3. We compare this carefully constructed test against the clustering evolution observed for the samples matched by number density. The passively evolving model that we test against was described in Section 4.

We fit an amplitude to the large-scale power-spectra at each redshift, as described in Section 3. We are interested in the evolution of this amplitude from high- to low-redshift, so we will plot ratios of these amplitudes. Fig. 10 shows this ratio as a function of limiting magnitude at high-redshift, for the luminosity-matched and number density matched samples as the black solid line and stars.

There are four distinct points to appreciate about Fig. 10:

(i) neither the luminosity-weighted nor the standard-weighted power-spectrum follow passive evolution at the faint end;

(ii) in both cases the most luminous objects are found to be consistent with passive evolution;

(iii) the departure from passive evolution is comparable in both cases; and

(iv) in both cases, there is an under-evolution of the power-spectrum amplitude with redshift, with respect to that expected from passive evolution.

The departure from passive evolution is less clear in the luminosity-weighted power-spectrum when we fit for shot-noise independently at high- and low-redshift (in the open black squares), which we do for the reasons given in Section 4. The general behaviour is, however, maintained. A clearer signal is at the moment not possible due to the limited redshift baseline given by our sample.

6   MODEL DEPENDENCE

Our results are naturally dependent on the choice of stellar model that describes the passive evolution of stellar colours and luminosity. We justify our choice of model by noting that it describes the *colour* evolution of at least a sub-sample of LRGs (those tested in Maraston et al. 2009) over a redshift range that goes beyond what is needed here. Implicitly, we assume that this model is a good description al *all* LRGs in our sample. In this section we explicitly discuss possible ways in which the modelling may be wrong.

The luminosity evolution, for one, is not as well constrained as the colour evolution. We must keep in mind that a model that would predict a different rate of stellar fading would impact on our weights that in turn would impact on the sample of galaxies that is returned by our matching scheme. The dominant factor in this case is the slope of the Initial Mass Function (IMF) at around $1M_\odot$ (Conroy et al. 2009), but there are in principle other reasons for a change

in the luminosity evolution. Although quantitatively motivated by changes to the IMF, the test we present in this section is general for all.

As explicitly demonstrated in Fig. 8 of Conroy et al. (2009), a change in the slope of the IMF of around ± 0.8 affects the expected B magnitude change of passively evolving galaxy by as much as 0.4 magnitudes for $z \lesssim 1$. The details of this calculation most certainly depend on the exact modelling of the passively evolving galaxy, as well as on the studied spectral region. However, we can certainly test for an error of this order of magnitude in our samples. We assume that the quoted uncertainty is uniformly distributed since $z = 1$ and that $|dM| = 0.2dz$. We therefore change Equation 1 to

$$M_{r,0.1} = r_p - 5\log_{10}\left\{\frac{D_L(z_i)}{10\mathrm{pc}}\right\} - Ke(z,0.1) \pm 0.2z \quad (25)$$

and re-run our analysis as before. For our redshift slices, which have approximately $dz = 0.15$, the introduced magnitude difference between high and low-redshift will be of the order of ± 0.03 magnitudes with respect to the assumed IMF slope. Note that what is important here is the *differential* effect with redshift, which affects galaxies in V_A and V_B with different degrees - we are insensitive to an overall shift in luminosity. In the case of a negative shift ($dM = -0.2dz$), galaxies at lower redshifts will have faded more with respect to galaxies at high-redshift, and we will need *more* objects in V_B to explain the luminosity in V_A. So whereas before we saw a deficit in the number density when matching the light, we should now find more closely matched number densities. The same reasoning applied to a positive shift ($dM = 0.2z$), means we should require fewer low redshift galaxies. Note that when we match by number density the main difference comes not from selecting different galaxies, but rather from a different evolution of the magnitudes of these galaxies. The reasoning is similar to the above - for a negative shift we expect the luminosity density at low redshift to be decreased with the respect to the fiducial model. So when we saw an excess in luminosity when matching by number density, we now expect this excess to be reduced.

We show the effect of a $\pm 0.2z$ change in the fiducial luminosity evolution on the ratios of number and luminosity densities, as well as growth rates, in Figs 7 and 8. In each case, the red ($dM = 0.2z$) and blue ($dM = -0.2z$) lines show the expected evolution of number and luminosity densities if the luminosity evolution was off by $\pm 0.2z$. One can see that if our description for the luminosity evolution was off by $-0.2z$, then we could just about reconcile the observations with the passive evolution scenario (except perhaps for our faintest sample). In other words, we would be enriching the low-redshift sample with more (lower-luminosity) objects. However, the galaxies removed or included by applying this evolutionary change have the lowest luminosities and are the least biased. This change will consequently also affect the amplitude of the clustering signal.. We show the power-spectrum evolution results in Fig. 10. The enrichment of V_B with lower-luminosity objects causes the amplitude of the clustering to be further reduced, as one would expect. Therefore, even though a potential error in the modelling of the luminosity evolution could perhaps explain the evolution of number and luminosity densities without departing from dynamical passive evolution, it could not explain the
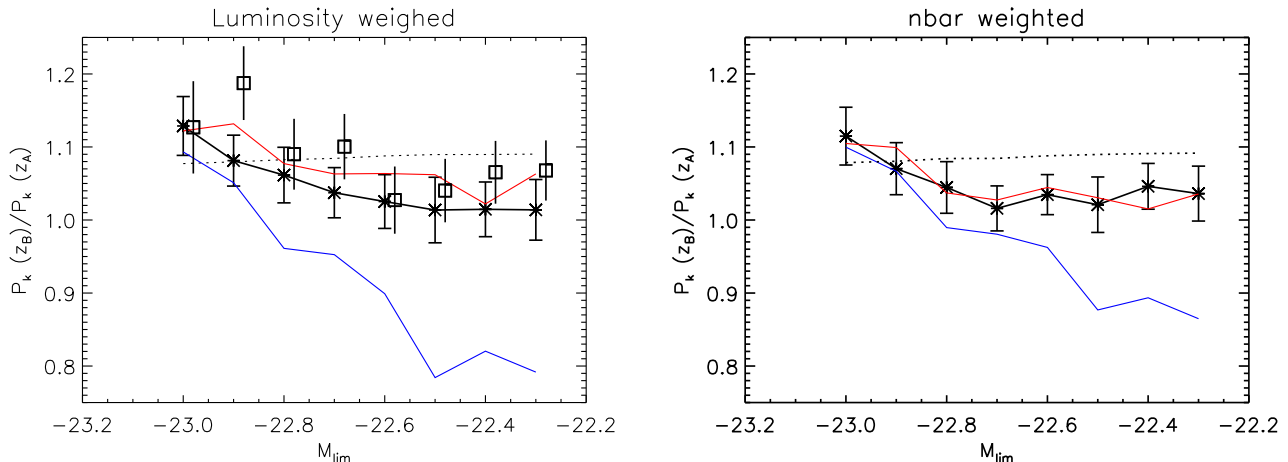
Figure 10. The ratio of the large-scale amplitude of the power-spectra at high- and low-redshift, as a function of the limiting magnitude at high-redshift. Left panel: luminosity-weighted samples and power-spectrum. Right panel: number density samples and uniformly-weighted power-spectrum. In both panels the dotted line shows the expected evolution from a pure passively evolving population of galaxies. The open squares in the left panel (slightly offset in magnitude for clarity) show the effect of fitting the shot noise separately, using a $k_{max} = 0.2$ - see Section 3 for details. The blue and red lines show the estimated effect of uncertainties in the IMF slope (see Section 6 for details). These data points are highly correlated, as each fainter sample includes the brighter ones.

evolution of the clustering. It is worth commenting on two further aspects of Figs 7, 8 and 10. In all cases, we see a stronger effect in the case of a $-0.2z$ shift, and one which increases to fainter magnitudes. This is probably explained by the slope in the luminosity function at low-redshift. By adding $-0.2z$, we are *adding* objects to the low-z sample (whilst keeping the high-z sample more or less the same - see next paragraph), and the results will depend heavily on the luminosity and number densities of these objects (which evolves faster towards fainter magnitudes). The other aspect worth mentioning is that we do not necessarily expect the blue and red lines to bound the solid black line in Fig. 10. In this case, the change in the results is given exclusively by the properties of the objects that either enter or leave the sample (with respect to the black line), and given that their number is small then this is effectively a noisy measurement. The exception is given by the increasing offset of the blue line, for which this number is in fact larger for the reasons mentioned above.

There is a final subtlety in the above analysis. When we apply Equation (25), we are effectively changing the absolute magnitude of all the objects in our sample. If we apply the same magnitude cuts as before, we then select a different sample of galaxies and comparison proves difficult. We therefore choose to shift the absolute magnitude limits at high-redshift by the same amount, in order to keep roughly the *same objects* in V_A for all cases. Note that both approaches would be valid - in one case we would be studying the effect of Equation (25) for fixed magnitude bins, and in the other we are studying the effect of Equation (25) on a fixed sample of galaxies.

We also do not directly address the question of contamination. As we find a clear deviation from passive evolution in at least part of our sample, we should keep in mind that this could very well be because the galaxies that reside in the lower-mass haloes are indeed not LRGs in the traditional, stellar population, sense of the word - i.e., their colours may

be mimicking those of LRGs due to dust, for example. This is perfectly OK - we are testing whether the galaxies that are selected according to the Eisenstein et al. (2001) target selection algorithm are passively evolving in a dynamical sense, independently of what causes their colour evolution. We must only worry that we have a good model for the description of its colour evolution with redshift.

Finally, let us also consider a scenario in which LRGs are generally passively evolving, but their formation epoch has a dependence on luminosity, or mass. This scenario is easily motivated by the literature, as several authors have found a dependence of mean age with luminosity in early-type galaxies (e.g. Caldwell et al. 2003; Thomas et al. 2005; Clemens et al. 2006), and would effectively mean that the M09 model, even if correct for the most massive LRGs, may become increasingly inadequate for fainter objects. However even the LRGs in our faintest sample, with $M_{r,0.1} > -22.3$, have typical masses of $10^{11.5} M_\odot$, and velocity dispersions greater than 200km s^{-1}. Given these numbers, we should expect a difference in formation age of less than 1Gyr, which would make little difference for the spectral evolution at the redshifts we are considering. This gives us confidence that the interpretation we present in the next section is driven by the dynamical evolution of the objects in our sample, rather than by an increasingly inadequate model as we go to fainter galaxies.

The dependence on the stellar model is characteristic of all studies that need to match LRG samples at low and high-redshift, and emphasises the importance of having a good model for the colour and luminosity evolution of LRGs.

7 INTERPRETATION

In Sections 5.1, 5.2 and 5.3 we have shown the results of testing passive evolution of LRGs using number and luminosity density evolution, as well as the evolution of the clustering

of LRGs. If our goal is to simply test dynamical passive evolution of LRGs, then our three measurements give a very clear answer - LRGs, as selected, do not *all* follow passive evolution. Fig. 7, 8, 9 and 10 consistently show evidence for merging of some sort. In all cases we also see a clear dependence on luminosity - the brightest galaxies show the smallest departure from pure passive evolution.

To explain the change in weighted number and luminosity densities seen in Fig. 7 and Fig. 8, we have to call in on some kind of merging scenario that explains the increasing luminosity density for samples with the same number density, or the decrease in the number of galaxies needed to explain the same amount of light. This can happen in three distinct ways:

(i) merging within the sample;
(ii) galaxies outside the sample merging with galaxies in the sample; or
(iii) galaxies outside the sample merging together and getting bright enough to make it into the sample.

The clustering result is the least clear, because of the relatively small redshift range probed. At the same time, however, the introduction of the luminosity-weighted power-spectrum has the most potential to tell us something about the nature of the evolution of LRGs, and differentiate between the three scenarios above.

If we restrict ourselves to the samples matched by number density and a uniformly-weighted power-spectrum, then our results are in agreement with previous work from White et al. (2007); Wake et al. (2008), where it was found that the evolution of the large-scale bias or clustering amplitude show very little evolution with redshift. A valid interpretation for this signal is the merging of objects at high-redshift into one LRG at low-redshift, which decreases the number density of objects in high-mass haloes and brings the large-scale clustering amplitude down.

However, if the evolution (or lack of) seen in the right-hand panel of Fig. 10 is explained by the merging of satellite LRGs within the sample, then we expect the luminosity-weighted power-spectrum to follow passive evolution. The fact that the data in the left-hand panel matches that in the right, showing some evidence for a departure from this hypothesis, leads us to consider a scenario where the lack of evolution in the large-scale power is due to *new* objects entering the sample between the two redshifts.

We can further assert how the new objects are entering the low-redshift sample. If the growth happens at the massive end, we expect the evolution of the power-spectrum to overshoot that expected from passive evolution, as more weight is given to objects that are intrinsically more strongly clustered. In reality, we observe the opposite behaviour. The only explanation that is consistent with both measurements is that objects in lower mass haloes are gaining weight from high to low redshift.

We cannot distinguish between a scenario where galaxies that fall completely outside the sample at high-redshift come together and become bright enough to make it into the sample at low-redshift, from a scenario where the faint end of the sample at high redshift is gaining weight from the merging of companions that initially fall outwith the sample. These two scenarios, however, are one and the same - *the growth of LRGs, as a population, is happening at the low mass end*. As we slide our magnitude limits we probe different regions of this growth but we observe it increases as we go down in halo mass/luminosity.

7.1   Intra-Cluster Light

We have so far ignored the possibility that light is lost in a merging event. If this happens then the luminosity-weighted power-spectrum is no longer expected to follow passive evolution in the case of merging within the sample. We can ask the question: is there a fraction of light loss per merger of given mass that can explain the observed lack of evolution in the luminosity-weighted power-spectrum? To answer this question quantitatively, we need to know how the amplitude of the power-spectrum changes as a function of luminosity, $P(k, L)$, which we leave for a follow-up paper.

Qualitatively however, we can still make the following observation: we need to increase the weight of objects residing in smaller haloes at low redshift to explain the observed deficit in power. It follows that any light loss at the bright end would have to be such that the resulting increase in luminosity of the bright objects is low enough that the clustering of these objects does not dominate the overall clustering signal. This would point towards a differential mass loss fraction with luminosity, with the most luminous objects losing the most mass to the ICM. The slope of this relation is related to the slope of $\partial P(k, L)/\partial L$, but we would still require preferential mass growth at the low-mass end - in fact, even more so. It therefore seems inevitable to conclude that the LRG growth is happening predominantly in lower mass haloes.

8   COMPARISON WITH PREVIOUS WORK

Our analysis has given us as a behavioural description of the growth of LRGs. Under our hypothesis, the luminosity growth that we present in Fig. 8 is being introduced by objects that live in smaller mass haloes, rather than satellite accretion into luminous central objects. This means that we cannot interpret the changes in number density between high and low redshift as a merger rate. The luminosity growth, in turn, is more directly comparable with previous results.

Even so, the comparison with other work is far from straightforward, given the different colour/luminosity selection, number density, redshift range and absolute magnitudes explored in each work. Most simply, we expect LRG growth to increase with redshift, and with decreasing luminosity. Table 8 presents a non-exhaustive collection of recent literature results that measured either the merger rate, or the luminosity growth rate of LRGs using a variety of techniques. The results that we present in Fig. 8 can at least be said to sample the same range of values in Table 8, with the exception of the growth measured by Masjedi et al. (2008). This may be reconciled with our interpretation if we consider that we need new objects becoming bright enough to become LRGs form high to low redshift and that is what dominates LRG growth. By cross-correlation LRGs with the main galaxy population, the authors concentrate only on the growth of existing LRGs.

Publication	Redshift range	Luminosity Growth (Gyr^{-1})	Merger rate (Gyr^{-1})	Number density (Mpc^{-3})
Masjedi et al. (2006)	0.16 - 0.36	-	0.6×10^4 Gpc^{-3}	-
Wake et al. (2006)	0.2 - 0.55	-	< 10 %	$\approx 1 - 25 \times 10^{-6}$
Brown et al. (2007)	< 0.9	$\approx 3\%$	-	$\approx 3 \times 10^{-4}$
White et al. (2007)	0.5-0.7	$< 18\%$	$\approx 3.4\%$	$\approx 10^{-3}h^3$
Cool et al. (2008)	0.1 - 0.9	$\approx 6.8\%$	-	$\approx 3 - 9 \times 10^{-5}$
Masjedi et al. (2008)	0.16 - 0.30	$< 1.7h\%$	-	-
Wake et al. (2008)	0.2 - 0.55	-	2.4 %	$\approx 3 \times 10^{-4}$
De Propris et al. (2010)	0.45 - 0.65	-	0.8×10^4 Gpc^{-3}	-

Table 4. A summary of the values obtained in the literature for the growth and merger rates of LRGs. These may be compared with the results we present in Table 3 and in Fig.8, but note the varying redshifts and number densities in each study.

The luminosity-weighted power-spectrum is a powerful tool to disentangle merging scenarios: mergers between satellites and centrals without light loss would give different evolution in the large-scale clustering strength between number density and luminosity matched catalogues. Instead we see similar evolution. Additionally, in order to match the observed decrement in the power spectrum evolution for the less-luminous galaxies and the increased rate of evolution in number and luminosity density, the simplest explanation is that LRGs need to be introduced in smaller haloes which are intrinsically less clustered. This interpretation is at odds with the one typically offered by the halo model, which is based on the small-scale clustering of samples not split by luminosity and that are matched by number density. In the "standard" halo-model based explanation, departures from passive evolution are due to satellite-central mergers. The need to match by number density when applying the halo model to test evolution is on itself a problem in performing these fits as, if the model suggests some fraction of satellites merge onto the central galaxy, then the number density at low redshift must also be reduced. How exactly to do this is not immediately obvious, and has been done differently by different authors.

9 DISCUSSION AND SUMMARY

We have, for the first time, applied luminosity weighting to sample selection and to the power-spectrum, and have presented a new method with which to interpret the evolution of LRGs. We have also introduced a new weighting scheme that allows us to keep most of the galaxies in the sample. This has allowed us to study the evolution of LRGs as a function of luminosity with unprecedented resolution. We have done this by measuring evolution of the number and luminosity density of SDSS LRGs with $0.15 < z < 0.5$, as well as the evolution of their clustering.

We can summarise our interpretation and conclusions in the following bullet points:

• The evolution of LRGs, as a population, is inconsistent with passive evolution.

• Departure from pure passive evolution is strongest for fainter LRGs; bright LRGs are consistent with pure passive evolution.

• We see a lack of evolution in the large-scale luminosity-weighted power spectrum for objects with $M_{r,0.1} \lesssim -22.8$, relative to what is expected from passive evolution. This effectively rules out option (i) in Section 7 as an explanation for the merger and luminosity growth rates presented in Table 3, although the evidence for this interpretation is not strong as a consequence of the relatively narrow redshift range probed.

• To explain this lack of evolution instead we propose that *LRGs in smaller mass haloes must gain weight (luminosity) since $z = 0.5$*. It is unclear whether options (ii) or (iii) of Section 7 are dominant, but given our sliding magnitude cuts the two are effectively the same process.

• Our interpretation relies on the assumption that light is conserved when two galaxies merge. However, even if this is not true, any weight given to LRGs in high-mass haloes must be offset by new objects in low-mass haloes entering the sample at $z < 0.5$. This, however, only increases the need to introduce less clustered objects into the low-redshift sample.

• Our results are not inconsistent with the halo model interpretation, nor previous work, if we restrict ourselves to the same observables. The added information in this paper comes from the matching of the samples on luminosity density (rather than number density) and on the evolution of the large-scale luminosity-weighted power-spectrum.

• We have explicitly estimated the effect of uncertainties in the IMF slope in the rate of fading of the stellar populations and in the subsequent selection and interpretation of our samples. The departure from passive evolution seen in the number and luminosity densities can certainly be attributed to an (extreme) uncertainty of the IMF slope. However, the resulting clustering signal is then clearly inconsistent with dynamical passive evolution.

.

In terms of pushing this analysis further, the Baryon Oscillation Spectroscopic Survey (BOSS; Schlegel et al. 2009), part of the SDSS-III project, will measure redshifts of LRGs out to $z < 0.7$. This will provide the lever-arm required to fully test the evolution of clustering strength as a function of redshift. When combined with luminosity-weighting this will allow us to test whether our interpretation is indeed correct.

REFERENCES

Blake C., Glazebrook K., 2003, ApJ, 594, 665
Blanton M. R., Roweis S., 2007, AJ, 133, 734
Brown M. J. I., Dey A., Jannuzi B. T., Brand K., Benson A. J., Brodwin M., Croton D. J., Eisenhardt P. R., 2007, ApJ, 654, 858
Brown M. J. I., Zheng Z., White M., Dey A., Jannuzi B. T., Benson A. J., Brand K., Brodwin M., Croton D. J., 2008, ApJ, 682, 937
Caldwell N., Rose J. A., Concannon K. D., 2003, AJ, 125, 2891
Carroll S. M., Press W. H., Turner E. L., 1992, ARAA, 30, 499
Clemens M. S., Bressan A., Nikolic B., Alexander P., Annibali F., Rampazzo R., 2006, MNRAS, 370, 702
Cole S., et al., 2005, MNRAS, 362, 505
Coles P., Jones B., 1991, MNRAS, 248, 1
Conroy C., Gunn J. E., 2009, ArXiv e-prints
Conroy C., Gunn J. E., White M., 2009, ApJ, 699, 486
Conroy C., Ho S., White M., 2007, MNRAS, 379, 1491
Cool R. J., Eisenstein D. J., Fan X., Fukugita M., Jiang L., Maraston C., Meiksin A., Schneider D. P., Wake D. A., 2008, ApJ, 682, 919
Davis M., Peebles P. J. E., 1983, ApJ, 267, 465
De Propris R., Driver S. P., Colless M., Drinkwater M. J., Loveday J., Ross N. P., Bland-Hawthorn J., York D. G., Pimbblet K., 2010, AJ, 139, 794
Eisenstein D. J., et al., 2001, AJ, 122, 2267
Feldman H. A., Kaiser N., Peacock J. A., 1994, ApJ, 426, 23
Fioc M., Rocca-Volmerange B., 1999, ArXiv Astrophysics e-prints astro-ph/9912179
Fry J. N., 1996, ApJL, 461, L65+
Górski K. M., Hivon E., Banday A. J., Wandelt B. D., Hansen F. K., Reinecke M., Bartelmann M., 2005, ApJ, 622, 759
Hamilton D., ed. 1998, The evolving universe. Selected topics on large-scale structure and on the properties of galaxies Vol. 231 of Astrophysics and Space Science Library
Hockney R. W., Eastwood J. W., 1981, Computer Simulation Using Particles
Hu W., Haiman Z., 2003, Phys. Rev. D, 68, 063004
Kaiser N., 1987, MNRAS, 227, 1
Maraston C., Strömbäck G., Thomas D., Wake D. A., Nichol R. C., 2009, MNRAS, 394, L107
Masjedi M., Hogg D. W., Blanton M. R., 2008, ApJ, 679, 260
Masjedi M., Hogg D. W., Cool R. J., Eisenstein D. J., Blanton M. R., Zehavi I., Berlind A. A., Bell E. F., Schneider D. P., Warren M. S., Brinkmann J., 2006, ApJ, 644, 54
Matsubara T., 2004, ApJ, 615, 573
Mihos J. C., Harding P., Feldmeier J., Morrison H., 2005, ApJL, 631, L41
Percival W. J., et al., 2001, MNRAS, 327, 1297
Percival W. J., et al., 2009, MNRAS, pp 1741–+
Percival W. J., Nichol R. C., Eisenstein D. J., Weinberg D. H., Fukugita M., Pope A. C., Schneider D. P., Szalay A. S., Vogeley M. S., Zehavi I., Bahcall N. A., Brinkmann J., Connolly A. J., Loveday J., Meiksin A., 2007, ApJ, 657, 51
Percival W. J., Verde L., Peacock J. A., 2004, MNRAS, 347, 645
Polarski D., Gannouji R., 2008, Physics Letters B, 660, 439
Press W. H., Teukolsky S. A., Vetterling W. T., Flannery B. P., 1992, Numerical recipes in C. The art of scientific computing
Reid B. A., et al., 2009, ArXiv e-prints
Schlegel D. J., et al., 2009, ArXiv e-prints
Seo H., Eisenstein D. J., 2003, ApJ, 598, 720
Smith R. E., Scoccimarro R., Sheth R. K., 2007, Phys. Rev. D, 75, 063512
Thomas D., Maraston C., Bender R., Mendes de Oliveira C., 2005, ApJ, 621, 673
Wake D. A., et al., 2006, MNRAS, 372, 537
Wake D. A., Sheth R. K., Nichol R. C., Baugh C. M., Bland-Hawthorn J., Colless M., Couch W. J., Croom S. M., de Propris R., Drinkwater M. J., Edge A. C., Loveday J., Lam T. Y., Pimbblet K. A., Roseboom I. G., Ross N. P., Schneider D. P., Shanks T., Sharp R. G., 2008, MNRAS, 387, 1045
White M., Zheng Z., Brown M. J. I., Dey A., Jannuzi B. T., 2007, ApJL, 655, L69